Correlation between structure and magnetic behavior of Fe-P amorphous alloys

A. García-Arribas,* M. L. Fdez-Gubieda, I. Orúe, and J. M. Barandiarán
Departamento de Electricidad y Electrónica, Universidad del País Vasco, Apartado Postal 644, 48080 Bilbao, Spain

J. Herreros
Departamento de Fisica Aplicada II, Universidad del País Vasco, Apartado Postal 644, 48080 Bilbao, Spain

F. Plazaola
Departmento de Electricidad y Electrónica, Universidad del País Vasco, Apartado Postal 644, 48080 Bilbao, Spain
(Received 13 February 1995; revised manuscript received 22 June 1995)

A series of $Fe_{100-x}P_x$ alloys ($x=11-22$) have been prepared by electrodeposition. Fully amorphous samples ($x=16-22$) have been investigated from both a magnetic and a structural point of view, in order to clarify the magnetic behavior of such alloys. Magnetization, Mössbauer, and extended x-ray-absorption fine structure (EXAFS) measurements (in both the Fe-K and P-K edges) have been performed. The concentration dependence of the saturation magnetization at 0 K, the isomer shift, and the mean hyperfine field have been obtained using the first two techniques and agree with previously reported data. The structural parameters obtained by EXAFS spectroscopy indicate no change in the Fe-Fe nearest-neighbor arrangement in the series and only a slight increase in the number of P atoms around Fe as the P content increases. We observe a T^2 temperature dependence of magnetization, indicative of itinerant rather than localized magnetism. The atomic disorder of the samples is discussed in terms of the shape of the hyperfine field distributions and the structural disorder parameters obtained in the fit of the EXAFS spectra, and can be related to the behavior of the spontaneous magnetization. The characteristic behavior of the Curie temperature, whose value remains nearly unchanged over the range of composition studied, can be explained as a cancellation of volume effects and electron transfer from P to the $3d$ band of Fe.

I. INTRODUCTION

In the last decades, numerous investigations on amorphous ferromagnetic alloys have been performed, a number of them on Fe-based systems. In order to achieve the amorphous state, it is necessary in almost every case that a metalloid enter the composition of the alloy. The role of the components in the structure and properties of such materials can be studied in an easier way on binary compounds such as Fe-B or Fe-P.

Although the usual way of fabricating metallic amorphous alloys is rapid quenching from the melt, the electrodeposition technique has revealed itself as a convenient method of preparation. Its most limiting factor is the relatively little choice of compositions that can be obtained. From a magnetic point of view, the most interesting alloys that can be prepared by this technique are those with phosphorus as the glass former. Only very recently has an amorphous NiCoB alloy been obtained by electrodeposition.[1]

$Fe_{100-x}P_x$ alloys have been extensively studied in a wide range of compositions ($x=0-50$) with samples obtained by electrodeposition,[2–12] melt quenching,[12–18] and other less common methods such as rf sputtering.[19,20] Different authors coincide in stating that the boundary between completely amorphous materials and partially crystalline ones is in the range of 13–15 at. % P. Samples containing less phosphorus have a mixture of amorphous and microcrystalline structure. The fraction of amorphous phase diminishes when the total phosphorus content is reduced. The structure of the microcrystals is a disordered solution of P in the Fe bcc lattice. When plotted as a function of the phosphorus content, the magnetic moment per metal atom reflects the change from an amorphous structure to a microcrystalline one. This is attributed to the change in the Fe coordination number from about 12 (amorphous) to 8 (bcc crystalline). This behavior of the magnetic properties of Fe-P alloys is quite in contrast to that of Co-P and Ni-P where, though a transition from amorphous to crystalline or partially crystalline materials does exist, the number of nearest neighbors does not change substantially and the magnetic properties do not show discontinuities. In the amorphous region the rate of decrease in the magnetic moment with phosphorus increase is the same for the three systems.[21] Dietz and co-workers have discussed this behavior in light of complementary theories, of Corb's coordination bond model, and Malozemoff's band-gap theory (Refs. 5, 21, 22 and references therein). Although they conclude that both theories seem to explain the different behaviors of Fe-P and the other two systems in the crystalline region, both fail to obtain the correct value for the slope of the linear decrease in the amorphous range. In both cases the effect of phosphorus is overestimated.

It is also noticeable in the Fe-P alloys that the Curie temperature (T_C) remains constant or changes very little with increasing P content (up to a value of 25% P approximately) in contrast with what happens in other materials such as amorphous Fe-B (Ref. 23) or Co-P.[24] Moreover, in samples obtained by melt quenching, the value of T_C increases (also very little) with the percent of P,[13–15] whereas in electrodeposited samples a decrease[3] or an insensitive[25] behavior has been reported. From 25% to higher phosphorus concentra-

tion, a continuous decrease in T_C is reported until the magnetic order in amorphous Fe-P disappears at a concentration of 50–55 % P (in electrodeposited and sputtered samples).[7,20]

The fundamental magnetic properties such as magnetic moment per atom and Curie temperature are mainly determined by the local environment of the metal atoms. Mössbauer spectroscopy has been extensively used to investigate this point and the Fe-P system has been the subject of numerous publications.[3,6–9,12,16–20,31] The most important parameters accessible with this technique are the mean hyperfine field and the isomer shift. In the range of compositions where the Fe-P alloys are completely amorphous ($x>14$), the mean value of the hyperfine field shows a linear decrease (Ref. 6 and references therein). In the low-concentration range, it deviates from this behavior in the same way as the magnetic moment does. The isomer shift shows a more complicated pattern. It continuously increases from $x=0$ to 25 where it begins to decrease (this is the same concentration at which T_C loses its constancy[7]).

Direct insight on short-range order was obtained by Logan[2] who studied the radial distribution functions extracted from x-ray-diffraction experiments. However, this technique can only provide an average of the different atomic environments present in the sample. His main result was the coordination number of iron atoms, which turned out to be of the order of 13.5. Hiltunen and co-workers have also obtained radial distribution functions in Fe-P amorphous alloys (complemented with Mössbauer spectroscopy) while investigating the differences in samples obtained by electrodeposition and melt spinning.[12]

The extended x-ray-absorption fine structure (EXAFS) is an atom-sensitive spectroscopy capable of measuring the coordination number and interatomic distances in materials. It has been used to study other amorphous systems such as Co-P (Ref. 26) and the more complicated FeCoSiB alloys.[27]

In this work we present a complete study of the short-range order on samples of intermediate composition in the amorphous range. We have performed EXAFS experiments on both edges Fe and P and have also carried out magnetic and Mössbauer measurements in the same samples to correlate the results with those reported previously in the literature.

II. EXPERIMENT

A series of samples was prepared by electrodeposition from aqueous solutions using a recipe based on the one published by Logan and Yung,[28] with compositions ranging from 11 to 22 at. % P. The deposition was performed at constant current onto polished copper substrates that were removed chemically after deposition. To avoid possible inhomogeneities occurring during preparation due to edge effects, only the central part of the deposit was used for the experiments. Thickness varied between 10 and 70 μm. The composition of the samples was determined by emission plasma spectroscopy and x-ray energy-dispersive analysis. Maximum possible error is 1 at. % P. Amorphicity was checked by x-ray diffraction with Cu K radiation and confirmed by the EXAFS spectra of the samples.

Measurements of the saturation specific magnetization

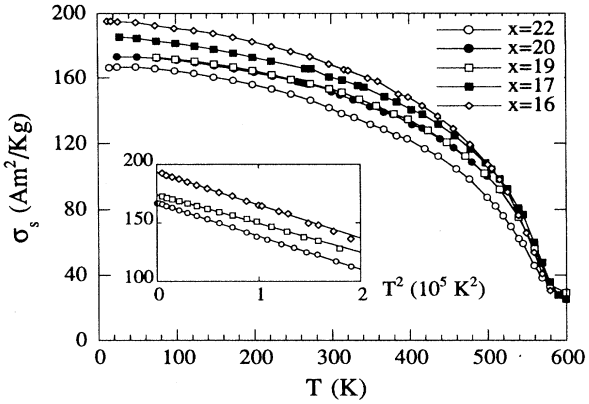

FIG. 1. Measured curves of specific magnetization as a function of the temperature. The tails in the vicinity of the Curie temperature are the onset of crystallization. The inset displays the fit of the low-temperature points to a T^2 law for some of the samples.

(σ_s) as a function of temperature were performed in a Faraday magnetometer between 25 and 750 K in fields up to 1200 KA m^{-1}. Mössbauer spectra were recorded at room temperature in a constant-acceleration spectrometer with a ^{57}Co-Rh source.

EXAFS experiments were performed at the Daresbury Laboratory Synchrotron facility running typically at 2 GeV and with an average current of 150 mA. The phosphorus K edge was measured in station 3.4 in total electron yield geometry using a double-crystal monochromator of InSb. The iron K edge was measured in station 7.1 in transmission geometry with a double-crystal Si(111) monochromator. All spectra were recorded at room temperature. Harmonic rejection is only necessary in the Fe edge, and it was achieved by detuning the monochromator to reduce the total intensity by 50%.

Samples with 14 at. % P and under show clear evidence of partial crystallinity in the x-ray and EXAFS spectra. The temperature behavior of the magnetization in the partially crystalline samples clearly deviates from the trend of the amorphous ones, and so we have restricted our study to completely amorphous samples ranging from 16 to 22 at. % P. The Fe K-edge EXAFS spectra of the sample $x=16$ could not be measured due to its excessive thickness. EXAFS spectra from the P K edge in samples $x=16$ and 17 were too noisy for data analysis.

III. DATA ANALYSIS AND RESULTS

A. Magnetization data

Figure 1 presents saturation magnetization versus temperature, $\sigma_s(T)$, curves for the samples studied. The spontaneous magnetization at 0 K, σ_0, has been obtained by extrapolating the σ_s-T^2 fitting of the points in the low-temperature range of the $\sigma_s(T)$ curves (inset of Fig. 1). Other temperature dependences were tried, such as σ_s-$T^{3/2}$, but the quality of the fitting was worse. This $T^{3/2}$ dependence is used in Ref. 25, but in the fitting presented there, it is clear that such a law is only followed in a small range of temperatures and not at the lowest ones. Therefore the T^2 depen-

TABLE I. Specific magnetization at 0 K and its correspondence in Bohr magnetons per Fe atom, and values of the Curie temperature as obtained from $\sigma(T)$ curves.

x	σ_0 (A m^2/Kg)	μ_{Fe} (μ_B)	T_C (K)
16	193	2.13	564
17	186	2.07	567
19	174	1.96	565
20	173	1.97	566
22	165	1.91	561

dence is a better description of the data. The values of σ_0 obtained by us show a linear increase with Fe content of about 15%, matching results reported previously by Dietz and co-workers.[21,22]

The Curie temperatures of the samples T_C are in the vicinity of the crystallization temperature, and so when the $\sigma_s(T)$ curve is measured slowly, as in this case, they crystallize before reaching T_C. To obtain the approximate value of T_C, we have to fit the points near T_C to a critical law of the form $\sigma_s \sim (T-T_C)^{\beta}$, with $\beta \sim 0.3$, and then extrapolate to $\sigma_s=0$. Other authors[3,25] have obtained the value of T_C from induction measurements, which is a faster method, with similar precision. Our results indicate a constant value of 564 ± 3 K for T_C and fall within the narrow interval of variation of T_C reported by Logan and Sun[3] for electrodeposited samples in the range of composition studied. Table I summarizes the results obtained for magnetization and Curie temperatures.

With the values of σ_0 and T_C so obtained, the universal curves σ_s/σ_0 vs T/T_C can be calculated for the samples studied. These reduced curves coincide exactly for $x=16$–20, while the one for $x=22$ is slightly depressed (see below).

B. Mössbauer data

The room-temperature Mössbauer spectra of all samples studied show a broad and asymmetric six-line pattern characteristic of amorphous ferromagnetic alloys (Fig. 2). The asymmetry has been attributed to the existence of anisotropic hyperfine fields[29] which appear in many other transition-metal amorphous alloys.

The data were fitted assuming a hyperfine field distribution (HFD) at Fe sites calculated by the smooth histogram procedure of Brand *et al.*,[30] where the quadrupole interaction is treated as a perturbation of the magnetic interaction and it is assumed to average to zero. A quite satisfactory fit of the experimental spectra is obtained assuming a linear correlation between the local magnetic hyperfine field B_{hf} and the local isomer shift (IS).

The relative intensity of line 2 or 5 with respect to line 3 or 4, $D23$, lies between 0.3 and 1 for x = 16,17,19,20. This indicates that the Fe magnetic moments align preferably parallel to the γ ray and so perpendicularly to the sample plane. This is a common feature of electrodeposited samples and is related to the way they grow. It is also apparent in the hysteresis loops,[31] although in the Fe-P alloys this perpendicular anisotropy is not so clear as in Co-P.[32] In contrast, the sample with $x=22$ shows an almost randomly distributed anisotropy

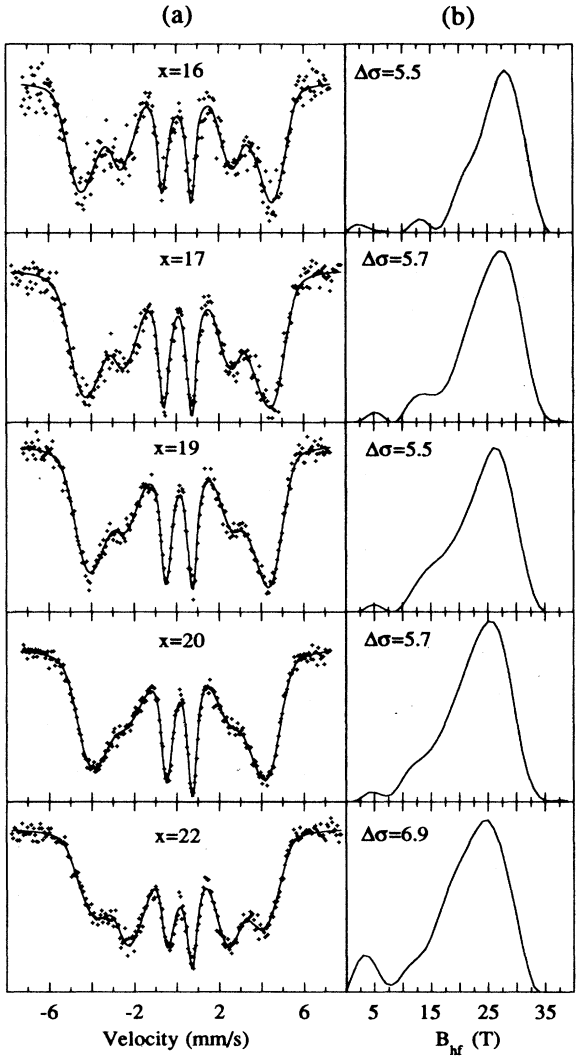

FIG. 2. (a) Mössbauer experimental and fitted spectra for $Fe_{100-x}P_x$ samples. (b) Hyperfine field distribution (HFD) found by the fitting program.

($D23=1.78$). Randomness of the magnetic moments in this sample was further checked by performing Mössbauer spectra in a sample tilted 45° from the direction of the incident of the γ ray. The change in the distribution of the magnetic anisotropy can be explained in terms of the morphology of growth without invoking structural changes. In fact, this last sample was the thinnest one (about 10 μm) and there is evidence in Co-P electrodeposited samples that the evolution of perpendicular anisotropy starts in the first stages of deposition with a preliminary in-plane anisotropy which evolves gradually toward a perpendicular position with increasing thickness.[33,34]

We have focused our interest on the results obtained for the average isomer shift relative to bcc iron at 300 K, IS, the mean hyperfine field, $\hat{B}_{hf}$, and the standard deviation $\Delta\sigma$ of the hyperfine field distribution, HFD, calculated as $\Delta\sigma=[\hat{B}^2_{hf}-(\hat{B}_{hf})^2]^{1/2}$. The first two are represented in Fig. 3. The mean value of the hyperfine field shows a linear de-

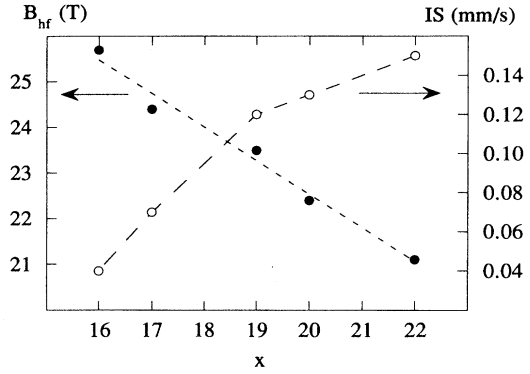

FIG. 3. Average hyperfine field and isomer shift as a function of composition for $Fe_{100-x}P_x$ samples.

creasing dependence on composition. Our values are nearly the same that those reported by Elsukov and co-workers in Ref. 7. However, they are lower than the ones reported previously by the same authors[6] and others.[12,20] These discrepancies are presumably connected to the way the mean values of the hyperfine field distribution are calculated, as discussed in Ref. 7. The isomer shift values show a monotonic increase and are also very similar to those reported previously.[7,12]

C. EXAFS data

Normalized EXAFS functions $\chi(k)$ were obtained using the standard procedure.[35] Absorption above the edge was fitted using a three-cubic spline in the k range $2 \leq k \leq 14$ Å^{-1} for the metal edge and a two-cubic spline in the range $2 \leq k \leq 9$ Å^{-1} for the phosphorus K edge. The presence in the spectra of a sulphur edge (due to the vacuum chamber contamination) reduced the effective EXAFS range in the P edge. The origin of k space was taken at the inflection point of the absorption edge.

$Fe_{100-x}P_x$ EXAFS functions obtained in this way are reported in Fig. 4(a) for the Fe K edge and in Fig. 5(a) for the P K edge. As can be seen in Fig. 4(a) the Fe K-edge $\chi(k)$ spectra of the samples studied differ strongly at low k values ($k \leq 6$ Å^{-1}). This is to be expected due to the fact that the P atoms scatter very strongly in the k range $3 \leq k \leq 5$ Å^{-1}. On the other hand, the $\chi(k)$ spectra for the P K edge seem to be very similar in all the samples studied [Fig. 5(a)].

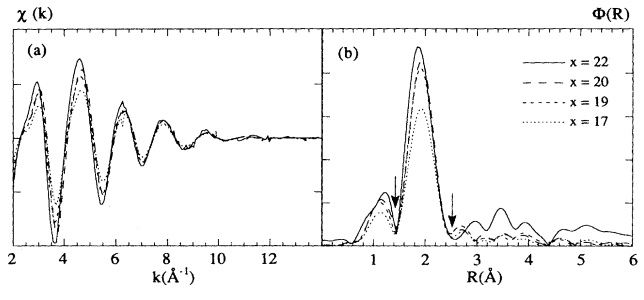

FIG. 4. (a) Fe K-edge EXAFS functions for $Fe_{100-x}P_x$ samples, $\chi(k)$. (b) Fourier transform of the EXAFS functions $\Phi(R)$. The arrows mark the width of the main peak used in the back Fourier transform.

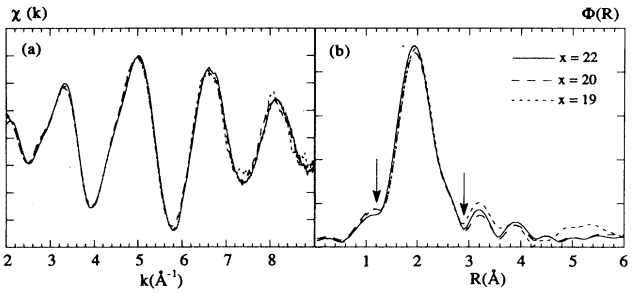

FIG. 5. (a) P K-edge EXAFS functions for $Fe_{100-x}P_x$ samples, $\chi(k)$. (b) Fourier transform of the EXAFS functions $\Phi(R)$. The arrows mark the width of the main peak used in the back Fourier transform.

The Fourier transform of $\chi(k)$ has been performed with a k^3 weight and a Hanning window function in the k range $2 \leq k \leq 14$ Å^{-1} for the metal edge and in the range $2 \leq k \leq 8$ Å^{-1} for the metalloid edge. All Fourier transforms present a single peak as can be seen in Figs. 4(b) and 5(b).

In order to remove noise from experimental data, an inverse Fourier transform was performed on the main peak [the range used is shown in Figs. 4(b) and 5(b)]. The so-filtered EXAFS function was then compared to a model function in a least-squares fitting routine. The range used for the fitting was the same for all samples, $3.5 \leq k \leq 11.5$ Å^{-1}. The goodness of the fit can be observed in Fig. 6, both in R and k space, for $Fe_{80}P_{20}$.

In the analysis of amorphous samples, a general approach in terms of the partial radial distribution function $g_j(r)$ (RDF) should be used. The EXAFS function is then given by

$$k\chi(k) = \sum_j f_j(k,\pi) e^{-2\sigma_j^2 k^2} \int \frac{e^{-2\Gamma_j/k}}{r^2} g_j(r) \sin[2kr + \phi_j(k)]\, dr. \quad (1)$$

Here $f_j(k,\pi)$ is the backscattering amplitude function of atoms of type j around the absorbing species, k is the photoelectron wave vector, ϕ_j is the total phase shift,

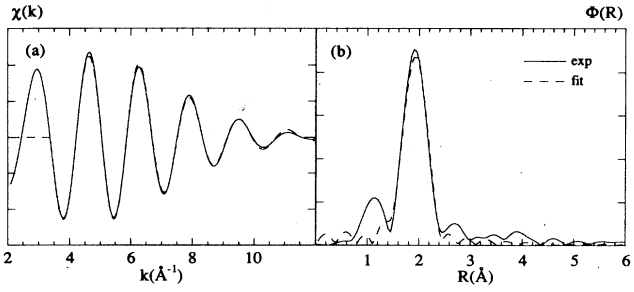

FIG. 6. Fe K-edge experimental and fitted EXAFS functions for $Fe_{80}P_{20}$, showing the quality of the fit in both k space (a) and (b) R space.

TABLE II. Structural parameters relative to the Fe K edge for the reference compounds bcc Fe and Fe_2P.

x	N_{FeFe}	R_{FeFe} (Å)	N_{FeP}	R_{FeP} (Å)
bcc Fe	8.1(5)	2.471(3)		
	5.8(6)	2.852(4)		
Fe_2P	1.3(8)	2.55(2)	1.3(4)	2.24(2)
	2.2(5)	2.67 (2)	0.8(4)	2.380(2)
	4(2)	2.692(1)	3(1)	2.48(2)
	2(2)	3.0(1)		

$\exp(-2\Gamma_j/k)$ is a mean-free-path term that takes into account the inelastic losses, and $\exp(-2\sigma_j k^2)$ is the Debye-Waller factor.

In the EXAFS analysis of data from highly disordered systems, the use of Gaussian radial distribution functions gives rise to a first-shell distance displaced to smaller r values than the actual interatomic distances obtained by x-ray and scattering measurements. The difference between EXAFS and x-ray-diffraction (XRD) results is attributed to the occurrence of a very asymmetrical nearest-neighbor distribution.[36–38] In the framework of a dense random packing of hard spheres (DRPHS) model,[39] Crescenzi *et al.*[40] proposed a RDF given by

$$g_j(r)=\begin{cases}\dfrac{1}{\sigma_{D_j}}e^{-(r-R_j)/\sigma_{D_j}} & \text{for } r\geq R_j,\\ 0 \quad \text{for } r<R_j,\end{cases} \tag{2}$$

where R_j is the distance between the centers of the two touching spheres and σ_{D_j} is the root-mean-square displacement giving the amount of structural disorder around its atomic site. The average distance will then be given by $\bar{R}=R_j+\sigma_D$. Using this expression, Eq. (1) can be integrated, giving

$$k\chi(k)=\sum_j N_j f_j(k,\pi)\frac{e^{-2\sigma_j^2k^2e^{-2\Gamma j/k}}}{R_j^2}\frac{1}{\sqrt{1+4k^2\sigma_{D_j}^2}} \times\sin[2kR_j+\tan^{-1}(2k\sigma_{D_j})+\phi_j], \tag{3}$$

where N_j is the number of atoms of j type around the absorbing one.

This expression has already been shown to give good results in other metallic glasses like $Co_{80}P_{20}$, $Ni_{80}P_{20}$,[26] and $Fe_{80}B_{20}$,[40,41] with good agreement between EXAFS and XRD results.

Model functions were built by a linear combination of Fe-Fe and Fe-P pairs for the Fe K edge. For the P K edge, we have considered only P-Fe pairs due to the fact that no metalloid-metalloid nearest neighbors have ever been reported in similar alloys.[42–44]

TABLE IV. Structural parameters relative to the P K edge for $Fe_{100-x}P_x$ amorphous samples.

x	N_{PFe}	R_{PFe} (Å)	$\sigma_{D_{PFe}}$ (Å)	$\bar{R}_{PFe}$ (Å)
19	8.2(9)	2.20(1)	0.14(2)	2.34(3)
20	8.6(9)	2.20(1)	0.14(2)	2.34(3)
22	9.2(9)	2.19(1)	0.15(2)	2.34(3)

Theoretical amplitudes and phase shifts were taken from FEFF3 codes.[45] Scattering factors have been optimized using bcc Fe and Fe_2P as reference compounds. The values obtained in the fitting of these compounds are included in Table II. The value of the Γ parameter is provided by the FEFF3 program.

Our analysis of the structural parameters has as starting point the results already found by diffraction techniques on samples with very similar composition: $Fe_{82}P_{18}$ (Ref. 46) and $Fe_{75}P_{25}$ (Ref. 47) ($\bar{R}_{FeFe}=2.61$ Å, $\bar{R}_{FeP}=\bar{R}_{PFe}=2.38$ Å, $N_{FeFe}=10.7$, $N_{FeP}=2.6$, $N_{PFe}=8.1$) where we have to take into account that these distances are average values. EXAFS spectroscopy is able to give more detailed results since it is more sensitive to closest distances R_j than to average distances $\bar{R}$.

The values of the best-fit parameters are presented in Tables III and IV. Very similar results[48] have been found using backscattering amplitudes and phase shifts from McKale calculations.[49] The error bar on each parameter was obtained by changing that particular parameter until its contribution to χ^2 doubles.[50] The definition of the minimized function, which is similar to the statistical χ^2 function, can be found in Ref. 51.

The environment of the phosphorus atom is very similar in all the samples studied. The interatomic distance $R_{PFe}=R_{FeP}=2.20\pm0.02$ Å is close to the sum of the covalent radii, indicating a covalent character of the bonds. Its coordination number $N_{PFe}=8.5\pm1$ is similar to that found by diffraction techniques. Due to the extremely restricted k range available for the P K edge, the coordination number has a large error bar. Nevertheless, bond distances are quite reproducible.

On the other hand, while the Fe-Fe coordination number is constant in all the samples and with the same value that is reported by diffraction techniques, $N_{FeFe}=10.2\pm0.5$, the number of P atoms around Fe increases, from 2 to 3, with an increasing P content, maintaining in all cases the stoichiometric relation. Although one can argue that the changes in the N_{FeP} values obtained from the fit are all within the experimental error, the increment of the number of P atoms in

TABLE III. Structural parameters relative to the Fe K edge for $Fe_{100-x}P_x$ amorphous samples.

x	N_{FeFe}	R_{FeFe} (Å)	$\sigma_{D_{FeFe}}$ (Å)	$\bar{R}_{FeFe}$ (Å)	N_{FeP}	R_{FeP} (Å)	$\sigma_{D_{FeP}}$ (Å)	$\bar{R}_{FeP}$ (Å)
17	10.3(5)	2.343(3)	0.31(1)	2.65(2)	2.1(6)	2.21(2)	0.17(6)	2.38(8)
19	10.2(6)	2.350(4)	0.26(1)	2.61(2)	2.3(6)	2.20(2)	0.18(6)	2.38(8)
20	10.2(5)	2.346(3)	0.25(1)	2.60(2)	2.5(6)	2.21(2)	0.17(6)	2.38(8)
22	10.2(6)	2.345(4)	0.23(1)	2.58(2)	3.0(6)	2.18(2)	0.23(6)	2.41(8)

the Fe neighborhood is real: It can be confirmed from the low-k behavior of the raw EXAFS spectra, as has been discussed before [see Fig. 4(a)].

The nearest Fe-Fe distance is also the same in all the samples studied ($R_{\mathrm{FeFe}}=2.35$ Å) and very similar to that already found in $Fe_{80}B_{20}$ [$R_{\mathrm{FeFe}}=2.30$ Å (Refs. 40 and 41)]. This value is smaller than the nearest-neighbor distance of 2.48 Å found for bcc Fe (twice the Goldschmidt radius of 1.24 Å for eightfold-coordinated Fe). If one considered the Goldschmidt radius as the atom size and used the asymmetrical distribution function of Eq. (2) (with parameters taken from Table III), a nearest-neighbor distance of 2.35 Å would imply that 35% of the atoms are "interpenetrating." In this connection it should be noted that our Fe-Fe distance is rather similar to the shortest distance obtained by x-ray diffraction in polycrystalline Fe_2B ($R_{\mathrm{FeFe}}=2.36$ Å).[52] In this compound 28% of nearest-neighbor atoms are at a distance smaller than the sum of Goldschmidt radii. Wong and Liebermann[44] studied the structure of the amorphous alloy $Ni_{66}B_{33}$ using multishell modeling, an approach different from ours, and found four Ni atoms (about 38% of nearest-neighbor atoms) at 2.24 Å, again a distance significantly smaller than the sum of Goldschmidt radii. In all these examples the reduced metal-metal distances merely reflect the changed bonding configuration brought about by the addition of the metalloid.

Finally, we have found a slight increase of structural disorder, $\sigma_{D_{\mathrm{FeFe}}}$, with decreasing P content, that gives rise to a small increase of the average interatomic distance (from $\bar{R}_{\mathrm{FeFe}}=2.58$ Å for $Fe_{78}P_{22}$ to $\bar{R}_{\mathrm{FeFe}}=2.65$ Å for $Fe_{83}P_{17}$). These average distances are very similar to those found by diffraction techniques for $Fe_{82}P_{18}$ (Ref. 46) and $Fe_{75}P_{25}$ (Ref. 47) ($\bar{R}_{\mathrm{FeFe}}=2.61$ Å).

IV. DISCUSSION

We begin by analyzing the dependence of magnetization on P concentration. As has been pointed out, the main effect of phosphorus is to reduce the Fe magnetic moment, while the Curie temperature remains unchanged.

EXAFS results show that, while the Fe-Fe coordination number does not vary ($N_{\mathrm{FeFe}}\approx 10$), the number of P atoms around Fe increases with P content, from $N_{\mathrm{FeP}}\approx 2$ to 3. In the framework of a rigid band model, this increase of the Fe-P coordination number could explain the magnetic behavior as due to an increase in electron transference from the $3p$ band of P to the $3d$ band of Fe, thus reducing the magnetic moment. This is also corroborated by the monotonic increase of the isomer shift with x, found by Mössbauer spectroscopy (Fig. 3). The increment in the number of P atoms in the neighborhood of a given Fe atom leads to an increase of the $3d$ electron density at Fe atoms via charge transfer from the P atom. Such an increase results in a stronger shielding of the external Fe s electrons ($3s+4s$), which leads to a reduction of the effective s electron density at the Fe nuclei, thus increasing the isomer shift.

This description assumes an itinerant nature of the magnetism in the samples. This approach is supported by the low-temperature dependence of magnetization, which has been shown to follow a T^2 law up to temperatures of $T\sim 0.8T_C$ (see inset of Fig. 1), which is typical of weak ferromagnetism or Invar alloys.

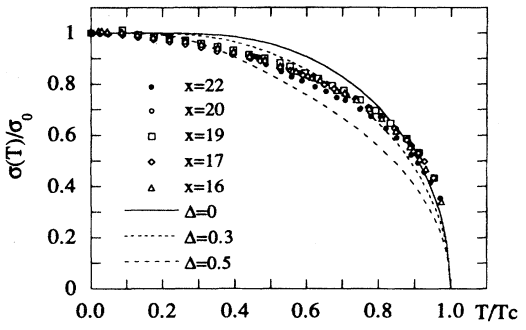

FIG. 7. Reduced magnetization curves calculated with Eq. (4) for different values of Δ and $S=\frac{1}{2}$ (see text). Experimental data from sample $x=22$ slightly deviates from the rest, and none of them coincide with the theoretical curves.

Some information about the short-range-order dependence on P concentration can be obtained from the analysis of the hyperfine field distribution HFD and the values of its standard deviation $\Delta\sigma$ presented in Fig. 2(b). The values of $\Delta\sigma$ are calculated taking the hyperfine field B_{hf} values in the range of 0–40 T. They are very similar for the samples with $x=16$, 17, 19, and 20 ($\Delta\sigma$ between 5.4 and 5.8 T), but $\Delta\sigma$ increases markedly in the last one, $x=22$ ($\Delta\sigma=6.9$ T). This is a consequence of the big contribution of a low-field peak appearing below $B_{\mathrm{hf}}=7$ T. This contribution has no significance for the rest of the samples, because when B_{hf} is restricted in the fit to the range of 7–40 T, the HFD obtained is only different for the sample with $x=22$. The other small peak that can be seen in the HFD at around 14 T in sample $x=16$ seems to evolve with increasing phosphorus content, entering the main peak as the latter displaces toward lower fields.

Taking into account the assumed proportionality between the hyperfine field B_{hf} and the Fe magnetic moment μ_{Fe}, the standard deviation of the hyperfine field distribution $\Delta\sigma$ becomes a measure of the width of the μ_{Fe} distribution. The finding of an increasing $\Delta\sigma$ would then imply a concomitant widening with P content of the distance distributions in the samples. However, from EXAFS data, the degree of disorder $\sigma_{D_{\mathrm{FeFe}}}$ is found to decrease slightly with increasing phosphorus content, from $\sigma_{D_{\mathrm{FeFe}}}=0.31$ for the sample with $x=17$ to $\sigma_{D_{\mathrm{FeFe}}}=0.23$ for $x=22$. In fact (Table III and Fig. 2), it is the disorder of the *Fe-P pairs* ($\sigma_{D_{\mathrm{FeFe}}}$) which correlates to $\Delta\sigma$. The influence of Fe-P pair disorder on the hyperfine field distribution is likely to be related to electron transfer variability due to different Fe-P local configuration and is consistent with the itinerant character of the magnetism already inferred by other means.

The reduced magnetization versus reduced temperature curves for the samples in the range $x=16$–20 coincide exactly, whereas for sample $x=22$ this curve is slightly depressed (see Fig. 7). On the basis of the molecular-field approach of Handrich,[53] a simple expression can be obtained for the reduced curve taking into account the fluctuations of the exchange integral due to structural disorder:[54]

$$\frac{\sigma_s(T)}{\sigma_0}=\frac{1}{2}\{B_s[(1+\Delta)x]+B_s[(1-\Delta)x]\}, \quad (4)$$

with

$$x=3\frac{S}{S+1}\frac{T_C}{T}\frac{\sigma_s(T)}{\sigma_0}, \quad (5)$$

where B_s is the Brillouin function and Δ is a measure of the degree of disorder, as defined in Ref. 54.

Though we have previously stated that an itinerant model is more suitable for the explanation of magnetic properties, from Eq. (4) (see Fig. 7), the main effect of disorder in such curves is to systematically depress them. As all our samples present very similar reduced curves, we can only deduce that the variations of disorder are to be small. Only the $x=22$ sample lies below the rest, indicating a slight increase in Δ. The exchange fluctuations can then be related to the disorder in the Fe-P pairs.

Finally, the dependence of the Curie temperature T_C on phosphorus content x can be explained on the basis of a phenomenological expression given by Luborsky, Walter, and Wohlfarth:[55]

$$\frac{dT_C}{dx}=\left(\frac{\partial T_C}{\partial x}\right)_V-\left(\frac{\partial T_C}{\partial P}\right)_x\frac{1}{KV}\frac{dV}{dx}+\left(\frac{\partial T_C}{\partial z}\right)_x\frac{dz}{dx}. \quad (6)$$

The first term gives the change of T_C with P content at constant volume V, arising from charge transfer from P to the Fe $3d$ band. The second term gives the influence on T_C of the volume effect, which derives from the change of the width of the Fe $3d$ band with the atomic volume. The last term in Eq. (6) relates T_C to the number of nearest-neighbor Fe atoms, z.

Luborsky *et al.* concluded from the study of a series of amorphous iron alloys that the size effect on T_C is small and the charge transfer effect is even less important. Thus the third term is the most relevant in determining the behavior of the Curie temperature. In our case we have found from EXAFS analysis that the Fe coordination number is nearly constant, $N_{\mathrm{FeFe}}\approx 10$, and so the Curie temperature behavior of these amorphous alloys must be determined by the contribution of the first two terms in Eq. (6). The reason why T_C does not change with composition is then related with the smallness of both terms as stated by Luborsky *et al.* and could be due to a compensation of the volume effects and the electron transfer from P to the $3d$ band of Fe. This would explain why the spontaneous magnetization changes while T_C does not change with composition. The fact that different preparation methods give rise to different T_C behaviors (increasing in melt spun and decreasing or insensitive in electrodeposited) could be related to slight structural differences induced by the preparation method, which have varying influences on the first two terms in Eq. (6).

V. CONCLUSIONS

From EXAFS data analysis in amorphous $Fe_{100-x}P_x$ ($17\leq x\leq 22$) samples, we have found that the Fe-Fe coordination number does not change, within the error, in the range studied, while the number of P atoms around Fe increases when increasing P content, from 2 to 3. Moreover, the Fe-Fe and Fe-P interatomic distances do not change in all the samples studied and only a slight increase of structural disorder has been found.

The evolution of the hyperfine field and exchange distributions with composition is related mostly to the disorder of the Fe-P pairs, as can be deduced from Mössbauer and magnetization measurements.

Structural parameters found by EXAFS spectroscopy allow us to explain the unusual behavior of the Curie temperature of $Fe_{100-x}P_x$ amorphous alloys, on the basis of an itinerant model deduced from a T^2 dependence of magnetization with temperature. It has been shown that such T_C behavior can arise from a compensation of charge transfer from P to the $3d$ band of Fe and volume effects on the width of the band.

ACKNOWLEDGMENTS

This work has been supported by the Spanish CyCIT under Grant No. MAT 93-0691. The authors wish to thank the Daresbury Laboratory for the use of its synchrotron facility, Dr. Javier Fernández Catuxo for EDX analysis of the samples, and Alberto Garcia for useful comments. One of the authors (I.O.) thanks the Basque Government for financial support.

*Permanent address: Dpto. de Física. Universidad de Oviedo, Av. Calvo Sotelo s/n, 33007 Oviedo, Spain.

[1] M. Onoda, K. Chimizu, T. Tsuchiya, and T. Watanabe, J. Magn. Magn. Mater. **126**, 595 (1993).
[2] J. Logan, Phys. Status Solidi A **32**, 361 (1975).
[3] J. Logan and E. Sun, J. Non-Cryst. Solids **20**, 285 (1976).
[4] G. Dietz and L. Börngen, J. Non-Cryst. Solids **58**, 275 (1983).
[5] F. Stein and G. Dietz, J. Magn. Magn. Mater. **81**, 294 (1989).
[6] E. P. Elsukov, Yu. N. Vorobev, A. V. Trubachev, and V. A. Barinov, Phys. Status Solidi A **117**, 291 (1990).
[7] E. P. Elsukov, Yu. N. Vorobev, and A. V. Trubachev, Phys. Status Solidi A **127**, 215 (1991).
[8] E. Kuzmann, S. Vitkova, Gy. Láng, G. Raichewski, and A. Vértes, Hyperfine Interact. **67**, 671 (1991).
[9] E. P. Yelsukov, Yu. N. Vorobyob, T. I. Arbusova, and I. B. Smolyak, J. Magn. Magn. Mater. **130**, 44 (1994).
[10] T. Osaka, M. Takai, A. Nakamura, and F. Asa, Denki Kagaku **82**, 453 (1994).
[11] K. Kamei and Y. Maehara, Mater. Sci. Eng. A **181/182**, 906 (1994).
[12] E. J. Hiltunen, J. A. Lehto, and L. Takacs, Phys. Scr. **34**, 239 (1986).
[13] M. Takahashi and M. Koshimura, Jpn. J. Appl. Phys. **16**, 2269 (1977).
[14] M. Mitera, M. Naka, T. Masumoto, N. Kazama, and K. Watanabe, Phys. Status Solidi A **49**, K163 (1978).
[15] N. S. Kazama, T. Masumoto, and M. Mitera, J. Magn. Magn. Mater. **15-18**,1331 (1980).
[16] D. Musser and C. L. Chien, J. Appl. Phys. **50**, 7659 (1979).
[17] M. Eibschütz, M. E. Lines, and H. S. Chen, Phys. Rev. B **28**, 425 (1983).
[18] K. Tanaka, N. Soga, K. Hirao, and K. Kimura, J. Appl. Phys. **60**, 728 (1986).

[19] R. L. McCally, J. S. Morgan, T. J. Kistenmacher, and K. Moorjani, J. Appl. Phys. **63**, 4124 (1988).
[20] R. L. McCally and K. Moorjani, J. Appl. Phys. **67**, 5784 (1990).
[21] K. Hüller, G. Dietz, R. Hausmann, and K. Kölpin, J. Magn. Magn. Mater. **53**, 103 (1985).
[22] F. Stein and G. Dietz, J. Magn. Magn. Mater. **117**, 45 (1992).
[23] M. Takahashi and M. Koshimura, Jpn. J. Appl. Phys. **16**, 1711 (1977).
[24] D. Pan and D. Turnbull, J. Appl. Phys. **45**, 1406 (1974).
[25] K. Hüller and G. Dietz, J. Magn. Magn. Mater. **50**, 250 (1985).
[26] P. Lagarde, J. Rivory, and G. Vlaic, J. Non-Cryst. Solids **57**, 275 (1983).
[27] M. L. Fdez-Gubieda, J. M. Barandiarán, F. Plazaola, A. Hernando, and S. Mobilio, J. Non-Cryst. Solids **151**, 51 (1992).
[28] J. Logan and M. Yung, J. Non-Cryst. Solids **21**, 151 (1976).
[29] G. Le Caer and J. M. Dubois, Phys. Status Solidi A **64**, 275 (1981).
[30] R. A. Brand, J. Lauer, and D. M. Herlach, J. Phys. F **13**, 675 (1983).
[31] A. García-Arribas, J. Herreros, J. M. Barandiarán, I. Orúe, and F. Plazaola, in *Proceedings of the IV International Workshop on Non-Crystalline Solids*, edited by M. Vazquez and A. Hernando (World Scientific, Singapore, 1995), p. 430.
[32] A. García-Arribas, J. M. Barandiarán, and J. Herreros, J. Magn. Magn. Mater. **131**, 129 (1994).
[33] G. C. Chi and G. S. Cargill III, in *Magnetism and Magnetic Materials*, edited by J. J. Becker, G. H. Lander, and J. J. Rhyne, AIP Conf. Proc. No. 29 (AIP, New York, 1976), p. 147.
[34] J. M. Riveiro and M. C. Sánchez, IEEE Trans. Magn. **MAG-15**, 1426 (1980).
[35] B. Lengeler and P. Eisenberger, Phys. Rev. B **21**, 4507 (1980).
[36] E. D. Crozier, J. J. Rehr, and R. Ingalls, in *X-Ray Absorption: Principles, Applications and Techniques of EXAFS, SEXAFS and XANES*, edited by D. C. Koningsberger and R. Prins (Wiley, New York, 1988), Chap. 9.
[37] P. Eisenberger and G. S. Brown, Solid State Commun. **29**, 481 (1979).
[38] R. Haensel, P. Rabe, G. Tolkiehn, and A. Werner, in *Liquid and Amorphous Metals*, edited by E. Lüscher and H. Coufal (Sijthoff and Nordhoff, Alphen aan den Rijn, The Netherlands, 1980), p. 232.
[39] J. L. Finney, Nature **266**, 309 (1977).
[40] M. Crescenzi, A. Balsatori, F. Comin, L. Incoccia, S. Mobilio, and N. Motta, Solid State Commun. **37**, 921 (1981).
[41] S. Mobilio and L. Incoccia, Nuovo Cimento **3**, 846 (1984).
[42] J. D. Bernal, Nature (London) **185**, 68 (1960).
[43] D. E. Polk, Scr. Metall. **4**, 117 (1970).
[44] J. Wong and H. H. Liebermann, Phys. Rev. B **29**, 651 (1984).
[45] J. Mustre de Leon, J. J. Rehr, R. C. Albers, and S. I. Zabinsky, Phys. Rev. B **44**, 4146 (1991).
[46] Y. Waseda and H. S. Chen, Phys. Status Solidi A **49**, 387 (1978).
[47] Y. Waseda, H. Okazaki, and T. Masumoto, in *The Structure of Non-Crystalline Materials*, edited by P. H. Gaskell (Taylor & Francis, London, 1977), p. 89.
[48] M. L. Fdez-Gubieda, A. García-Arribas, J. M. Barandiarán, and J. Herreros, Physica B **208&209**, 363 (1995).
[49] A. G. McKale, B. W. Veal, A. P. Paulikas, S. K. Chan, and G. S. Knapp, J. Am. Chem. Soc. **110**, 3763 (1988).
[50] S. Pascarelli, F. Boscherini, S. Mobilio, A. R. Zanatta, F. C. Marques, and I. Chambouleyron, Phys. Rev. B **46**, 6718 (1992).
[51] F. W. Lytle, D. E. Sayers, and E. A. Stern, Phys. Rev. B **158**, 701 (1989).
[52] R. W. G. Wycoff, *Crystal Structure* (Wiley, New York, 1964), Vol. II.
[53] K. Handrich, Phys. Status Solidi **32**, K55 (1969).
[54] J. Chappert, in *Magnetism of Metals and Alloys*, edited by M. Cyrot (North-Holland, Amsterdam, 1982), pp. 511–516.
[55] F. E. Luborsky, J. L. Walter, and E. P. Wohlfarth, J. Phys. F **10**, 59 (1980).